Rapid Communications

Measurements of single-state and state-ensemble lifetimes of high-lying Rb Rydberg levels

M. Archimi,[1] C. Simonelli,[1,2] L. Di Virgilio,[1] A. Greco,[1] M. Ceccanti,[1] E. Arimondo,[1,2] D. Ciampini,[1,2] I. I. Ryabtsev,[3,4] I. I. Beterov,[3,4,5] and O. Morsch[1,2,*]

[1]*Dipartimento di Fisica "E. Fermi", Università di Pisa, Largo Bruno Pontecorvo 3, 56127 Pisa, Italy*

[2]*INO-CNR, Via G. Moruzzi 1, 56124 Pisa, Italy*

[3]*Rzhanov Institute of Semiconductor Physics SB RAS, Novosibirsk State University, 630090 Novosibirsk, Russia*

[4]*Novosibirsk State University, 630090 Novosibirsk, Russia*

[5]*Novosibirsk State Technical University, 630072 Novosibirsk, Russia*

(Received 3 July 2019; published 4 September 2019)

We demonstrate a hybrid method based on field ionization and state-selective deexcitation capable of measuring the lifetimes of high-lying Rydberg levels. For nS Rydberg states of Rb atoms with principal quantum number $60 \leqslant n \leqslant 88$, we measure both the lifetimes of single target states and those of the ensembles of Rydberg states populated via blackbody-radiation-induced transitions. We find good overall agreement with numerical calculations of the expected lifetimes in both cases. However, for the target-state lifetimes, we find a local deviation towards shorter lifetimes for states around $n = 72$, which we interpret as a signature of a modified blackbody spectrum in the finite volume in which our experiments take place.

DOI: 10.1103/PhysRevA.100.030501

Rydberg states of atoms are characterized, amongst other properties [1,2], by long radiative lifetimes. Compared to low-lying excited atomic states, which typically decay on timescales of less than a microsecond, high-lying Rydberg states (with principal quantum number above $n \approx 50$) can live for hundreds of microseconds. This makes them attractive for applications, e.g., in quantum simulation and quantum computation [3], where the ground state and a Rydberg state can be used to encode quantum bits. In those applications, it is important also to take into account another peculiarity of high-lying Rydberg states, which is their interaction with blackbody radiation [4–8]. The resulting transition rates to other nearby Rydberg states can be comparable to or even larger than those due to spontaneous decay to low-lying states. This creates practical problems when measuring Rydberg state lifetimes, as the different Rydberg states populated by blackbody radiation are close in energy and, therefore, can be difficult to distinguish experimentally.

So far, a number of studies have addressed the issue of Rydberg state lifetimes [9–16]. Experimentally, different techniques such as field ionization and state-selective field ionization [17–19], trap loss spectroscopy [20], monitor states [15], and all-optical methods based on probe beam absorption have been used [16]. For alkali-metal atoms such as rubidium, which we use in the present study, lifetimes have been measured up to principal quantum numbers around $n = 45$ [15], and good agreement with numerical calculations has been found. For higher n, the typically employed methods become increasingly difficult to apply. State-selective field ionization for high-lying states above $n \approx 60$ requires one to distinguish states whose ionization thresholds differ only by a few percent (for instance, between the $80S$ and $81S$ states, it changes by 5% from 9.18 to 8.72 V/cm, and the values for the nearest $n'P$ states are even closer). Other techniques may also be unable to reliably measure the population of an individual Rydberg state, and instead only give information on a range of closely spaced Rydberg levels.

Here, we demonstrate a hybrid field ionization and state-selective laser deexcitation method that allows us to measure, in principle, the lifetimes of single Rydberg states for almost arbitrary principal quantum numbers (limited essentially by the linewidth of the deexcitation laser and by residual electric fields) as well as the lifetimes of the corresponding "state ensembles", i.e., of all Rydberg states that are populated by blackbody radiation starting from the initially excited state, called the "target state". Our measurements for nS Rydberg states with principal quantum numbers between 60 and 88 show good overall agreement with numerical calculations for both lifetimes. However, for the target-state lifetime, we find a local deviation from theory towards shorter lifetimes around $n = 72$, which we discuss in the context of the blackbody spectrum inside the finite volume of our vacuum cell.

In our experiments, we excite nS Rydberg states of ^{87}Rb atoms in a standard magneto-optical trap (MOT) containing around 200 000 atoms at temperature $T \approx 150\,\mu$K in a roughly spherical cloud 300 μm in size (Gaussian width; for details of the apparatus see [21,22]). The Rydberg states are reached from the $5S_{1/2}(F = 2)$ ground state via the intermediate $6P_{3/2}(F = 3)$ state using two copropagating laser beams at 420 and 1013 nm, with blue detuning $\Delta/2\pi = 37$ MHz of the 420 nm laser from the $5S_{1/2}(F = 2)$-$6P_{3/2}(F = 3)$ resonance (in each experimental cycle, the MOT beams are switched off for 1500 μs a few hundred nanoseconds before the excitation pulse, while the magnetic field remains switched on). Rydberg atoms are then detected by field ionization, in which a high-voltage pulse is applied to two pairs of electrodes placed outside the glass vacuum cell and the resulting ions are

*Corresponding author: morsch@df.unipi.it

accelerated towards a channel electron multiplier. The overall detection efficiency is around 40%, and the highest electric fields achievable in our apparatus correspond to the field ionization threshold for Rb Rydberg states with $n \approx 60$. We have checked that above that threshold the detection efficiency is largely independent of n.

A combination of field ionization and state-selective deexcitation [23] now gives us access to two quantities, as shown schematically in Fig. 1(a). After laser excitation of an initial Rydberg target state, a first measurement consists in waiting a variable time t after the excitation pulse (typical duration around 300 ns) and then applying the electric field ionization pulse. During the waiting time two processes take place: spontaneous decay of atoms in the target state primarily to low-lying states because of the interplay between increasing transition frequency and decreasing dipole moment with increasing Δn (around 95% of the atoms decay to states with n between 5 and 17, calculated using [24]), and absorption as well as stimulated emission of photons of the blackbody radiation inside the glass cell, which populates nearby Rydberg states with principal quantum number n' and angular momentum L (from which, in turn, other nearby states can be populated in a multistep process [8]). While atoms that have undergone spontaneous decay can no longer be field ionized, those that have exchanged photons with the blackbody radiation typically end up in states that are detected as Rydberg states in field ionization. We now fit an exponential decay to the measured number of Rydberg atoms $N_{\mathrm{ens}}(t)$ [see Fig. 1(b)] and call the resulting $1/e$-time τ_{ens} the state-ensemble lifetime. Given the practical constraints, the "state ensemble" denotes all Rydberg $n'L$ states that can be field ionized in our experiment.

The second measurement is similar to the first one, except that before field ionization, a 5 μs deexcitation laser pulse with Rabi frequency $\Omega/2\pi$ between 2 and 4 MHz resonantly couples the target Rydberg state to the $6P_{3/2}(F = 3)$ intermediate state. This is achieved by changing the frequency of a double-pass acousto-optic modulator in the beam path of the 1013 nm laser, whereby the frequency of the deexcitation pulse can be suddenly (within 100 ns) increased by 37 MHz, matching the detuning $\Delta/2\pi$ of the excitation pulse. The $6P_{3/2}$ state has a lifetime of 120 ns, so effectively the deexcitation laser pulse depumps target state atoms to the ground state. After the deexcitation pulse, field ionization as described above measures the number of Rydberg atoms left in the cloud. In the case of a 100% depumping efficiency α, only atoms that have been redistributed out of the target state to nearby Rydberg states, which are not resonant with the deexcitation pulse, will contribute to the field ionization signal (in practice, α is around 95%, and the duration of the pulse is chosen to be much shorter than the expected target-state lifetime, whilst still resulting in a reasonable depumping efficiency). We call these states the "support" of the target state, and a typical measurement of the support population $N_{\mathrm{supp}}(t)$ is shown in Fig. 1(b).

From $N_{\mathrm{ens}}(t)$ and $N_{\mathrm{supp}}(t)$ we can now infer the number of atoms in the target Rydberg state $N_{\mathrm{tar}}(t)$ from the relations $N(t) = N_{\mathrm{ens}}(t) = N_{\mathrm{tar}}(t) + N_{\mathrm{supp}}(t)$ (before depumping) and $N'(t) = (1-\alpha)N_{\mathrm{tar}}(t) + N_{\mathrm{supp}}(t)$ (after depumping). Fitting an exponential decay to $N_{\mathrm{tar}}(t)$, we obtain τ_{tar}. A typical

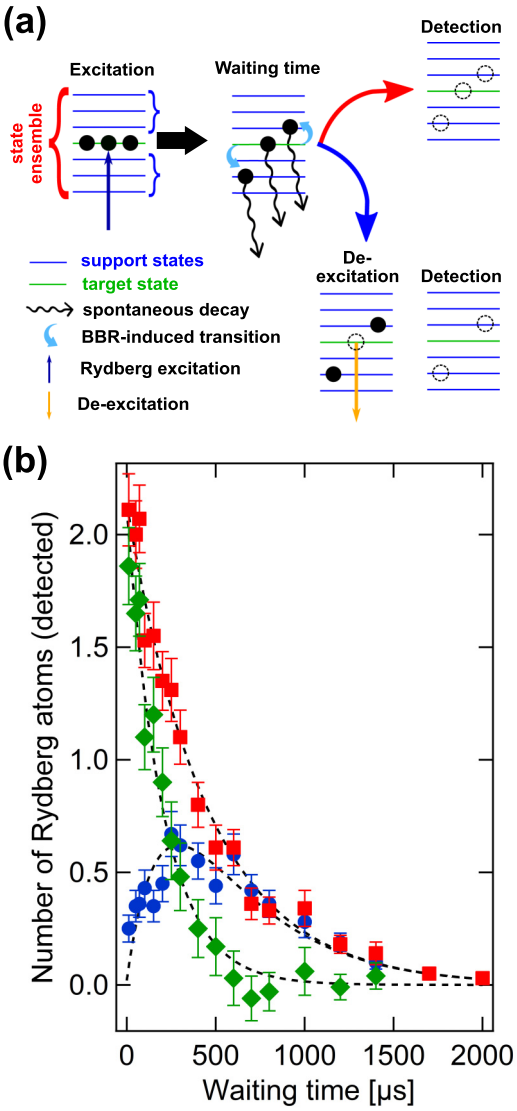

FIG. 1. Measurement of Rydberg target-state and state-ensemble lifetimes. (a) Schematic of the measurements. After excitation of the target state, the number of excitations in the state ensemble is measured by simple field ionization. The number of excitations in the support states, by contrast, is measured by first depumping the target state atoms to low-lying states using a 5 μs laser pulse resonant with the $6P_{3/2}(F = 3)$ state, and then field ionizing the remaining excitations. (b) A typical measurement of the number of Rydberg excitations in the state ensemble (red squares) and support states (blue circles) as a function of time for the 80S target state. The number of excitations in the target state (green diamonds) is then calculated from the difference of the state ensemble and support states. The dashed lines are exponential fits, from which the target-state and state-ensemble lifetimes are extracted (for the support data, the difference of the exponential fits for the state ensemble and target was calculated). Error bars are one standard error of the mean.

measurement of τ_{tar} for the 80S state is shown in Fig. 1(b). We note that for the target-state lifetimes reported in this work, the free fall and expansion of the atomic cloud between the excitation and depumping pulses (which leads to a decrease in the overlap between the spatial distribution of Rydberg atoms and the deexcitation beam) is not a substantial limitation, but

could be relevant for lifetimes exceeding 1000 μs (we discuss this in more detail later).

In principle, with our technique it is possible to measure target-state populations as long as the closest S or D states (which can be coupled to the $6P$ state by the deexcitation laser) are separated in energy from the target state by more than the linewidth of the deexcitation laser (around 500 kHz in our apparatus, including residual Doppler broadening). In practice, however, there are further limitations. First, van der Waals interactions (which are responsible for the well-known dipole blockade effect [25,26]) or dipole-dipole interactions between Rydberg atoms (which can arise, for instance, between nS and $n'P$ states) can shift the target-state energy levels, resulting in an effective detuning of the deexcitation laser and hence a variation in the depumping efficiency α over time, which will lead to systematic errors in the inferred lifetime. In order to limit such effects, we adjusted the two-photon Rabi frequency and duration of the excitation pulse such as to excite only $\approx$4 Rydberg atoms on average (corrected for the detection efficiency) in a cloud defined by the overlap between the MOT and the two excitation lasers with waists 40 μm (420 nm laser) and 90 μm (1013 nm laser). The mean spacing between two Rydberg atoms (assuming a uniform distribution inside the cloud) was, therefore, on the order of 50 μm, and hence van der Waals and dipole-dipole interactions could, to first approximation, be neglected (for instance, the van der Waals interaction between two $70S$ atoms at that distance is less than 100 Hz).

A second limitation of our technique stems from electric fields in the vacuum cell, to which Rydberg atoms are extremely sensitive due to their large polarizability, which scales roughly as n^7. From measurements of the Stark map (target nS state and the $(n-3)$ Stark manifold) and comparison with numerical calculations [24], we determined the background electric field in our cell to be 215 ± 10 mV/cm (the error includes day-to-day fluctuations). This field is likely due to rubidium atoms adsorbed on the inner surface of the cell (and possibly charge buildup during the experimental cycle, which becomes evident when the repetition rate is increased much beyond 10 Hz), charged dust particles on the outside of the cell, and other field sources whose origin we are unable to establish with certainty. By applying a few tens of volts to the field ionization electrodes we were able to compensate a part of the background field, leading to a minimum residual field of around 100 mV/cm.

To study the effect of a finite electric field E on our lifetime measurements, we measured the target-state and state-ensemble lifetimes as a function of E (Fig. 2). In particular, we scanned the electric field around the Inglis-Teller limit, for which the $(n-3)$ Stark manifold crosses the nS target state (the value of E was deduced with an error of around 10% from a measurement of the Stark map). Below the Inglis-Teller limit, both target-state and state-ensemble lifetime agree with the theoretical predictions. From Fig. 2, two main effects are evident. Most strikingly, around the Inglis-Teller limit the observed target-state lifetime drops by two orders of magnitude to a few microseconds and remains low for larger E. The state-ensemble lifetime, by contrast, shows no particular variation at the Inglis-Teller limit but a distinct increase for larger field values.

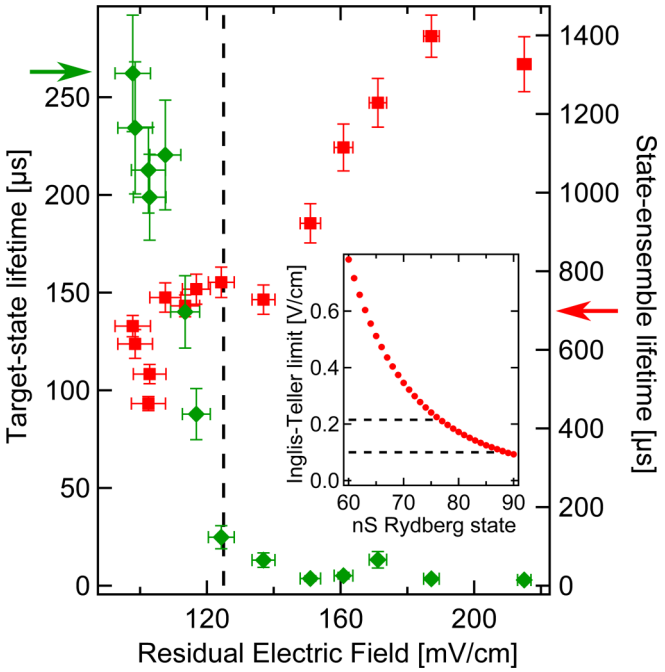

FIG. 2. Effect of the residual electric field E in the cell on the measured target-state (green diamonds) and state-ensemble lifetimes (red squares). Below the Inglis-Teller limit for the $85S$ state used here (vertical line), both lifetimes agree with the theoretical predictions (arrows) of 258 μs for the target state and 719 μs for the state-ensemble lifetime. Error bars are one standard error of the mean (for the electric field values, we estimate an error based on our measurement protocol). Inset: The Inglis-Teller limit for the range of principal quantum numbers considered in this work (calculated using [24]). The dashed horizontal lines indicate the electric field in the cell with (bottom) and without compensation (top).

While the increase of the state-ensemble lifetime above the Inglis-Teller limit can be explained by the fact that the central states of the $(n-3)$ Stark manifold with large angular momentum, and hence longer lifetime, are mixed into the target nS state, at present we have no simple physical picture for the drastic behavior of the target-state lifetime. One possible explanation might be electric field inhomogeneities and state changes at the avoided crossings in the Stark manifold due to atomic motion, which could lead to a variation of the depumping efficiency α over time. However, thus far we have not been able to experimentally verify that hypothesis.

From the above discussion, we conclude that in the absence of interaction effects between Rydberg atoms, our measurement protocol allows us faithfully to deduce the target-state and state-ensemble lifetimes for Rydberg states with an Inglis-Teller limit greater than the 100 mV/cm residual electric field in our cell (see inset of Fig. 2), and hence an upper limit of $n = 88$. In Fig. 3 we report the measured lifetimes [27] for states with $60 \leqslant n \leqslant 88$ (the lower limit is due to the upper limit of our ionization field). In order to compare our results with theoretical predictions, we used a numerical model taking into account both spontaneous decay as well as blackbody-induced population redistribution at $T = 300$ K between the ensemble Rydberg states (taking into account states up to $L = 3$), including the possibility of a repopulation of the target

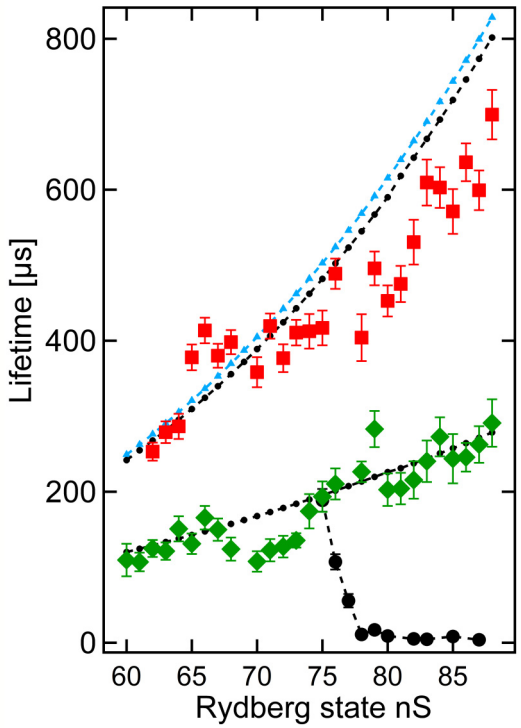

FIG. 3. Measurement of target-state (green diamonds) and state-ensemble lifetimes (red squares) of high-lying Rb Rydberg states. The small black circles (connected by dashed lines to guide the eye) are the results of numerical simulations of the coupled blackbody repopulation and spontaneous decay processes. The small blue triangles (connected by dashed lines) represent the target-state lifetime at zero temperature. The large black circles (connected by a dashed line to guide the eye) are the target-state lifetimes without compensation of the electric field in the cell (that field is around 215 mV/cm, corresponding to the Inglis-Teller limit for the 76*S* state; for the other measurements in this figure the residual electric field in the cell was less than 90% of the Inglis-Teller limit). Note that for $n = 60$ and $n = 61$ no measurement for the state-ensemble lifetime is reported, as the lower limit of $n = 60$ for reliable field ionization leads to systematic errors, but states below $n = 60$ can be populated by blackbody radiation. Error bars are derived from the exponential fit.

state from the support states. The latter process leads to an observed target-state lifetime that is slightly longer (up to 10%) than the values usually quoted in the literature, which only take into account the departure from the target state due to blackbody-induced transitions. We find good agreement between the numerical calculation and our measurements for the target states, with a slight exception around $n = 72$ (which we will discuss below). In Fig. 3 we also report the target-state lifetimes measured without the electric field compensation; in that case, a sharp drop in the observed lifetime occurs around $n = 76$, above which the Inglis-Teller limit is below the uncompensated background field.

Using our numerical model we can also calculate the expected state-ensemble lifetimes and find reasonable agreement with our experimental results. Obviously, the state-ensemble lifetimes are considerably longer (up to a factor of 3) than the target-state lifetimes, as they are due to multistep blackbody redistribution processes to higher angular momentum states inside the state ensemble (either with or without a change in n), along with spontaneous decay, for which the lifetimes become longer as the angular momentum increases. From those calculations we find that in our experiments starting from nS states, during the evolution of the system P, D, and F states are significantly populated (i.e., more than a few percent of the total population), whereas higher angular momentum states can be neglected. Intuitively, right after the excitation of the target state, one expects the decay rate of the state ensemble to be dominated by spontaneous decay of the target state to low-lying states, whereas all other processes leave the state-ensemble number unchanged. The state-ensemble lifetime should, therefore, approximate the Rydberg state lifetime at zero temperature. From Fig. 3 it is evident that the simulation for the state-ensemble lifetimes confirms this, and the experimental results also support that interpretation.

We now turn to the discrepancies between our experimental results and the numerical calculations. For the target-state lifetimes, there is a localized deviation with lifetimes shorter than expected by up to 25% around $n = 72$, for which the transition frequencies to nearby nP and $(n-1)P$ states are around 10 GHz. One reason for that deviation could be the presence of microwave radiation at those frequencies (owing to the large dipole moment of those transitions, microwave fluxes in the tens of pW/cm^2 regime would be sufficient to cause the observed deviation). In preliminary experiments [28], for which we added additional field electrodes to better compensate the background field, we were able to rule this out as a possible cause by shielding the apparatus with aluminum foil. (Using Autler-Townes splitting of the 91*S* state coupled to the 90*P* state induced by an external microwave source, we measured a shielding factor of around 4.)

This leaves a variation in the blackbody spectrum itself as a plausible explanation (other possible causes for enhanced decay, such as superradiance [29–32], are unlikely to play a role in our system due to the small number of excitations involved and the narrow range of parameters for which such effects are expected to occur in multilevel systems [33]). In fact, it is well known that the assumptions made in the derivation of the Planck formula for blackbody radiation are no longer valid when the wavelength of the radiation becomes comparable to the size of the blackbody, as the density of modes is strongly modified close to the longest-wavelength modes supported by the cavity [34–36] (signatures of such an effect were detected experimentally in [37]). The dimensions of our vacuum cell (internal cross section 1.8 cm×2.4 cm, with a thin coating of adsorbed Rb atoms on the inner walls) and of the surrounding support structures and coils are of the order of a few centimeters. The wavelengths corresponding to the transitions from nS states with $70 \leqslant n \leqslant 75$ to the closest $n'P$ states are between 2.5 and 3.3 cm and, therefore, comparable to those expected for the lowest modes inside the low-quality factor cavity formed by the glass cell. In addition, blackbody radiation stemming from the surrounding support structures can also be altered compared to the Planck formula due to finite-size effects, further modifying the expected blackbody spectral intensity seen by the Rydberg atoms. In principle, this could be modeled using the approach of [34,35], which would

involve calculating the modes and respective polarizations of the electromagnetic field both inside the cell and in the far field of nearby objects, taking into account the exact shapes of all the objects.

Regarding the state ensemble, we find deviations of up to 30%, particularly towards shorter lifetimes for $n > 70$, but also towards longer lifetimes. Again, these deviations might be partly due to the presence of microwave radiation with a spectral intensity that differs from the predictions of the Planck formula. Furthermore, as the state-ensemble lifetimes are several hundred microseconds, and hence measurements were taken up to several milliseconds, systematic effects due to the expansion and free fall of the atomic cloud might lead to an underestimation of the state-ensemble lifetimes. We have checked that the presence of the MOT lasers after 1500 μs (which are switched back on in order to minimize losses from the MOT during the experimental cycle, which is repeated at a frequency of 4 Hz, and keep the number of atoms constant) does not influence the measurements.

In conclusion, we have presented a method for measuring single-state and state-ensemble lifetimes of high-lying Rydberg states based on a hybrid field ionization and optical deexcitation technique. The measured lifetimes are in good overall agreement with numerical calculations. Our method is suitable for measuring subtle deviations from the theoretically predicted lifetimes due to, for instance, finite-size modifications of the blackbody spectrum or other effects such as super- or subradiance. In future experiments we plan to investigate the observed deviations more closely and to extend our measurement protocol to P, D, and F states, which will give us further insight into possible modifications of the blackbody spectrum.

We thank Thomas Gallagher, József Fortágh, Markus Greiner, David Petrosyan, Nikola Šibalić, Levi Schächter, and Darrick Chang for discussions, and Alessandro Tredicucci and Giorgio Carelli for the loan of microwave equipment. This work was funded by the H2020-FETPROACT-2014 Grant No. 640378 (RYSQ). I.I.R. and I.I.B. were supported by the Russian Foundation for Basic Research under Grant No. 17-02-00987 (for lifetime calculations), by the Russian Science Foundation under Grant No. 18-12-00313 (for multistep transitions induced by blackbody radiation), and by Novosibirsk State University.

[1] T. Gallagher and R. Atoms, *Cambridge Monographs on Atomic, Molecular and Chemical Physics* (Cambridge University Press, Cambridge, UK, 1994).

[2] R. Löw, H. Weimer, J. Nipper, J. B. Balewski, B. Butscher, H. P. Büchler, and T. Pfau, An experimental and theoretical guide to strongly interacting Rydberg gases, J. Phys. B: At. Mol. Opt. Phys. **45**, 113001 (2012).

[3] M. Saffman, T. G. Walker, and K. Mølmer, Quantum information with Rydberg atoms, Rev. Mod. Phys. **82**, 2313 (2010).

[4] T. F. Gallagher and W. E. Cooke, Interactions of Blackbody Radiation with Atoms, Phys. Rev. Lett. **42**, 835 (1979).

[5] J. W. Farley and W. H. Wing, Accurate calculation of dynamic Stark shifts and depopulation rates of Rydberg energy levels induced by blackbody radiation. Hydrogen, helium, and alkali-metal atoms, Phys. Rev. A **23**, 2397 (1981).

[6] W. E. Cooke and T. F. Gallagher, Effects of blackbody radiation on highly excited atoms, Phys. Rev. A **21**, 588 (1980).

[7] I. I. Beterov, I. I. Ryabtsev, D. B. Tretyakov, and V. M. Entin, Quasiclassical calculations of blackbody-radiation-induced depopulation rates and effective lifetimes of Rydberg nS, nP, and nD alkali-metal atoms with $n \leqslant 80$, Phys. Rev. A **79**, 052504 (2009).

[8] I. I. Beterov, D. B. Tretyakov, I. I. Ryabtsev, V. M. Entin, A. Ekers, and N. N. Bezuglov, Ionization of Rydberg atoms by blackbody radiation, New J. Phys. **11**, 013052 (2009).

[9] T. F. Gallagher, S. A. Edelstein, and R. M. Hill, Radiative lifetimes of the S and D Rydberg levels of Na, Phys. Rev. A **11**, 1504 (1975).

[10] C. A. Kocher and C. E. Fairchild, Time-of-flight determination of radiative decay rates for high Rydberg states in atomic nitrogen, J. Chem. Phys. **68**, 1884 (1977).

[11] W. A. Chupka, Factors affecting lifetimes and resolution of Rydberg states observed in zero-electron-kinetic-energy spectroscopy, J. Chem. Phys. **98**, 4520 (1993).

[12] F. Merkt and R. N. Zare, On the lifetimes of Rydberg states probed by delayed pulsed field ionization, J. Chem. Phys. **101**, 3495 (1994).

[13] A. L. De Oliveira, M. W. Mancini, V. S. Bagnato, and L. G. Marcassa, Measurement of Rydberg-state lifetimes using cold trapped atoms, Phys. Rev. A **65**, 031401 (2002).

[14] Z. G. Feng, L. J. Zhang, J. M. Zhao, C. Y. Li, and S. T. Jia, Lifetime measurement of ultracold caesium Rydberg states, J. Phys. B: At. Mol. Opt. Phys. **42**, 145303 (2009).

[15] D. B. Branden, T. Juhasz, T. Mahlokozera, C. Vesa, R. O. Wilson, M. Zheng, A. Kortyna, and D. A. Tate, Radiative lifetime measurements of rubidium Rydberg states, J. Phys. B: At. Mol. Opt. Phys. **43**, 015002 (2010).

[16] M. Mack, J. Grimmel, F. Karlewski, L. Sárkány, H. Hattermann, and J. Fortágh, All-optical measurement of Rydberg-state lifetimes, Phys. Rev. A **92**, 012517 (2015).

[17] T. F. Gallagher, L. M. Humphrey, R. M. Hill, and S. A. Edelstein, Resolution of $|m_l|$ and $|m_j|$ Levels in the Electric Field Ionization of Highly Excited d States of Na, Phys. Rev. Lett. **37**, 1465 (1976).

[18] P. Nosbaum, A. Bleton, L. Cabaret, J. Yu, T. F. Gallagher, and P. Pillet, Anticrossing spectroscopy of Cs Rydberg states, J. Phys. B: At. Mol. Opt. Phys. **28**, 1707 (1995).

[19] U. Hollenstein, R. Seiler, H. Schmutz, M. Andrist, and F. Merkt, Selective field ionization of high Rydberg states: Application to zero-kinetic-energy photoelectron spectroscopy, J. Chem. Phys. **115**, 5461 (2001).

[20] J. O. Day, E. Brekke, and T. G. Walker, Dynamics of low-density ultracold Rydberg gases, Phys. Rev. A **77**, 052712 (2008).

[21] M. Viteau, J. Radogostowicz, A. Chotia, M. G. Bason, N. Malossi, F. Fuso, D. Ciampini, O. Morsch, I. I. Ryabtsev, and E. Arimondo, Ion detection in the photoionization of a Rb Bose-Einstein condensate, J. Phys. B: At. Mol. Opt. Phys. **43**, 155301 (2010).

[22] M. Viteau, J. Radogostowicz, M. G. Bason, N. Malossi, D. Ciampini, O. Morsch, and E. Arimondo, Rydberg spectroscopy of a Rb MOT in the presence of applied or ion created electric fields, Opt. Express **19**, 6007 (2011).

[23] C. Simonelli, M. Archimi, L. Asteria, D. Capecchi, G. Masella, E. Arimondo, D. Ciampini, and O. Morsch, Deexcitation spectroscopy of strongly interacting Rydberg gases, Phys. Rev. A **96**, 043411 (2017).

[24] N. Šibalić, J. D. Pritchard, C. S. Adams, and K. J. Weatherill, ARC: An open-source library for calculating properties of alkali Rydberg atoms, Comput. Phys. Commun. **220**, 319 (2017).

[25] L. Béguin, A. Vernier, R. Chicireanu, T. Lahaye, and A. Browaeys, Direct Measurement of the van der Waals Interaction between Two Rydberg Atoms, Phys. Rev. Lett. **110**, 263201 (2013).

[26] E. Urban, T. A. Johnson, T. Henage, L. Isenhower, D. D. Yavuz, T. G. Walker, and M. Saffman, Observation of Rydberg blockade between two atoms, Nat. Phys. **5**, 110 (2009).

[27] For simplicity, we fit single exponential curves to our data in order to extract a single value for the lifetime, although the decay process is not perfectly exponential due to the many different transition and decay rates involved. In practice, however, we find that such a fit is typically a reasonable approximation.

[28] M. Archimi *et al.* (unpublished).

[29] M. Gross, P. Goy, C. Fabre, S. Haroche, and J. M. Raimond, Maser Oscillation and Microwave Superradiance in Small Systems of Rydberg Atoms, Phys. Rev. Lett. **43**, 343 (1979).

[30] T. Wang, S. F. Yelin, R. Côté, E. E. Eyler, S. M. Farooqi, P. L. Gould, M. Koštrun, D. Tong, and D. Vrinceanu, Superradiance in ultracold Rydberg gases, Phys. Rev. A **75**, 033802 (2007).

[31] T. Zhou, B. G. Richards, and R. R. Jones, Absence of collective decay in a cold Rydberg gas, Phys. Rev. A **93**, 033407 (2016).

[32] D. D. Grimes, S. L. Coy, T. J. Barnum, Y. Zhou, S. F. Yelin, and R. W. Field, Direct single-shot observation of millimeter-wave superradiance in Rydberg-Rydberg transitions, Phys. Rev. A **95**, 043818 (2017).

[33] R. T. Sutherland and F. Robicheaux, Superradiance in inverted multilevel atomic clouds, Phys. Rev. A **95**, 033839 (2017).

[34] A. M. García-García, Finite-size corrections to the blackbody radiation laws, Phys. Rev. A **78**, 023806 (2008).

[35] A. Reiser and L. Schächter, Geometric effects on blackbody radiation, Phys. Rev. A **87**, 033801 (2013).

[36] V. Fernández-Hurtado, A. I. Fernández-Domínguez, J. Feist, F. J. García-Vidal, and J. C. Cuevas, Super-Planckian far-field radiative heat transfer, Phys. Rev. B **97**, 045408 (2018).

[37] I. M. Beterov and I. I. Ryabtsev, Induced emission from a sodium Rydberg atom in a microwave cavity, JETP Lett. **69**, 448 (1999).